Rare Met. (2020) 39(5):513–528
https://doi.org/10.1007/s12598-019-01306-2

RARE METALS
www.editorialmanager.com/rmet

Recent progress in ceramic matrix composites reinforced with graphene nanoplatelets

Bei-Ying Zhou, Sheng-Jie Fan, Yu-Chi Fan, Qi Zheng, Xin Zhang, Wan Jiang, Lian-Jun Wang*

Received: 20 February 2019 / Revised: 28 April 2019 / Accepted: 20 June 2019 / Published online: 3 September 2019

Abstract Graphene nanoplatelets (GNPs) are considered to be one of the most promising new reinforcements due to their unique two-dimensional structure and remarkable mechanical properties. In addition, their impressive electrical and thermal properties make them attractive fillers for producing multifunctional ceramics with a wide range of applications. This paper reviews the current status of the research and development of graphene-reinforced ceramic matrix composite (CMC) materials. Firstly, we focused on the processing methods for effective dispersion of GNPs throughout ceramic matrices and the reduction of the porosity of CMC products. Then, the microstructure and mechanical properties are provided, together with an emphasis on the possible toughening mechanisms that may operate. Additionally, the unique functional properties endowed by GNPs, such as enhanced electrical/thermal conductivity, are discussed, with a comprehensive comparison in different ceramic matrices as oxide and non-oxide composites. Finally, the prospects and problems needed to be solved in GNPs-reinforced CMCs are discussed.

Keywords Graphene nanoplatelets; Ceramic matrix composites; Processing methods; Mechanical properties; Functional properties

B.-Y. Zhou, Y.-C. Fan, X. Zhang, W. Jiang, L.-J. Wang*
Engineering Research Center of Advanced Glasses Manufacturing Technology, Ministry of Education, Donghua University, Shanghai 201620, China
e-mail: wanglj@dhu.edu.cn

B.-Y. Zhou, Y.-C. Fan, W. Jiang
Institute of Functional Materials, Donghua University, Shanghai 201620, China

S.-J. Fan, Q. Zheng, L.-J. Wang
State Key Laboratory for Modification of Chemical Fibers and Polymer Materials, College of Materials Science and Engineering, Donghua University, Shanghai 201620, China

W. Jiang
School of Material Science and Engineering, Jingdezhen Ceramic Institute, Jingdezhen 333000, China

1 Introduction

Owing to the high hardness and strength, chemical inertness, low thermal conductivity, good oxidation and corrosion resistance, monolithic ceramics are widely used in traditional industrial sectors such as machinery, chemical engineering and metallurgy as promising structural materials. Very recently, they become increasingly popular in the fields of optoelectronics, biomedicine and aerospace. However, they still suffer from the inherent brittleness, mechanical unreliability and poor electrical conductivity [1–3]. This issue is particularly serious when the ceramic materials contain the glass phase, as the amorphous structure cannot provide any obstacle to crack propagation and the fracture toughness is really low (< 1 MPa·m$^{1/2}$) [4].

Since the pioneering work of Niihara in the 1990s [5], who added nanoparticles, nanofibers and whiskers as a second phase to ceramic matrix, ceramic matrix composites (CMCs) have become one of the most promising ways to improve the mechanical properties of monolithic ceramics. In addition, the reinforcing phase also benefits other properties such as hardness, thermal shock resistance, electrical conductivity, and thermal expansion coefficient. The combination of these characteristics with intrinsic advantages of ceramic matrix makes CMCs yield

substantial promise for advanced technologies such as hypersonic engines and aircraft, lightweight and high-lifetime prosthetics, and high-temperature electronic components, where other materials (e.g., metallic alloys) cannot be used effectively under such harsh conditions [6, 7].

The preparation of stable graphene nanoplatelets (GNPs) was reported by Geim et al. [8]. They used tapes to directly strip the graphite crystals. This method has attracted unprecedented attention and provided a new opportunity for the development of CMCs. The two-dimensional (2D) structure of GNPs yields a higher specific surface area of 2630 $m^2 \cdot g^{-1}$ than either CNTs or graphite, and the sp2 hybrid bonding of carbon atoms in GNPs is responsible for its exceptional properties, i.e., transmittance of 97.7%, in-plane elastic modulus of 0.5–1 TPa, tensile strength of 130 GPa, breaking strength of 42 $N \cdot m^{-1}$, electrical conductivity of 1×10^7 $S \cdot m^{-1}$ and thermal conductivity of 5300 $W \cdot m^{-1} \cdot K^{-1}$ [9–17]. In addition, flat morphology of GNPs provides more interfaces with ceramic matrix on both sides, unlike CNTs that only the exterior surface can form interfaces, thereby entailing more transformations of electrons, phonons and dissipations of energy in CMCs. For example, GNPs are more apt to survive in high-pressure processing than the tubular CNTs that encounter the problems of buckling and cracking [18, 19].

The aim of this article is to provide a comprehensive picture of the current advances in GNPs-reinforced CMCs. In this paper, a variety of methods employed for incorporating GNPs into ceramic matrices and consolidation techniques for fabricating bulk CMCs are discussed. An in-depth discussion on significant improvements in toughness and flexural strength, along with enhancements in electrical conductivity and thermal conductivity, is emphasized at the same time. In this part, the most widely studied GNPs–CMCs systems are classified according to the types of ceramic matrices as oxide and non-oxide composites. The toughening mechanisms and effects of GNPs on mechanical behavior and functional properties of CMCs are thoroughly discussed. Finally, prospects for future research needed to successfully harness the promise of GNPs-reinforced CMCs are provided based on the observed advantages and disadvantages of CMCs thus far.

2 Preparation process

2.1 Mechanical mixing

The GNPs at nanometric scale possess the intrinsic tendency to agglomerate due to van der Waals forces, a consequence of high surface area and high aspect ratio of GNPs, inducing a difficulty in obtaining uniform dispersion of GNPs. It is worth noting that uniform distribution of GNPs within ceramic matrix ensures efficient load transfer and stress distributions from ceramic matrix to GNPs, thus minimizing the presence of stress concentration points [20–22]. In an ideal situation, a fully densified ceramic composite with perfect GNPs dispersion without any damage and agglomeration in the ceramic matrix is required to achieve excellent performance of GNPs–CMCs. Therefore, various techniques are required to improve the dispersion of GNPs and processing routes need to be modified carefully and validated thoroughly to produce GNPs–CMCs.

Ball milling is a popular approach for mixing GNPs and ceramic powder ascribing to the high shear forces that not only can disperse but also reduce the number of stacked graphene layers by exfoliating. Hence, the ball milling process has been adopted to maximize the load sharing and pullout effect of graphene as it brings more interfaces between GNPs and ceramic matrix. Moreover, ball milling is a simple, scalable and cost-effective process and has been demonstrated to yield almost no contamination in the final powders by using tungsten carbide jars and milling balls [23, 24]. He et al. [25] firstly showed the relationship between the morphology of GNPs and ball milling time using a planetary ball mill with Al_2O_3 powder. The rotation speed steadied at 250 $r \cdot min^{-1}$ with a powder-to-ball ratio of 1:30. With the milling time increasing, the majority of the graphite sheets were broken, some exfoliations of GNPs occurred, and the sizes of the GNPs were reduced and became thinner. The GNPs with the smallest thickness of 3–4 nm can be produced after 30-h ball milling, while crumpling, rolling and damaging of the graphene sheets would happen after longer ball milling time. By adopting a sudden heating (1000 °C, 60 s, under a nitrogen atmosphere) to expand the graphite along its planes, Fan et al. [26] synthesized GNPs and Al_2O_3 ceramic mixture powder by planetary ball milling for longer durations when GNPs can be exfoliated more easily. Liu et al. [27] directly ground the graphite simply expanded by microwave heating with Al_2O_3 ceramic matrix using planetary mill for 30 h, which realized the exfoliation and reduction of expanded graphite, formation and dispersion of graphene nanosheets (GNSs) in one step (Fig. 1). Al_2O_3 ceramic composites homogeneously dispersed with GNSs were obtained by this method, in which the thickness of GNSs was mostly distributed in the range of 2-20 nm. Kun et al. [28] homogeneously distributed the multilayered graphene additives into Si_3N_4 ceramic by milling in a highly efficient attritor mill equipped with zirconia agitator delta disks and zirconia grinding media in silicon nitride tank. This milling process was performed at a high rotation speed of 3000 $r \cdot min^{-1}$ for 4.5 h. Attributing to the decrease in the agglomeration quotient of graphene during the high-energy

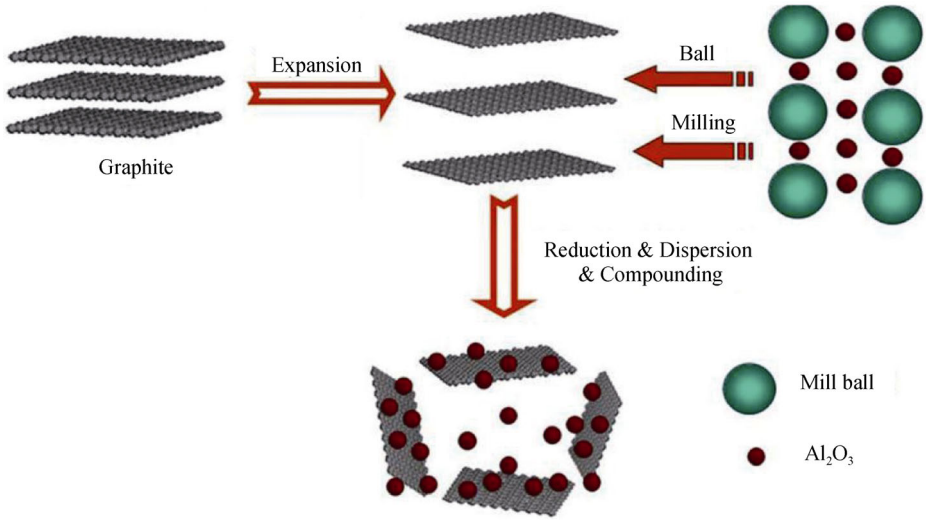

Fig. 1 Schematic illustration of exfoliation and dispersion of GNSs in Al_2O_3 ceramic [27]

mixing, a cumulative effect conferred from the increased graphene content was observed in improving the mechanical properties. However, the contained zirconia as contamination can hardly be avoided from media and disks.

Magnetic stirring and ultrasonication are other commonly used routes of producing graphene and ceramic matrix with homogenous dispersion and controllable properties based on colloidal chemistry. Typically, slow mixing favors the uniform dispersion of graphene into the ceramic matrix in similar solvent to ensure uniform dispersing medium [29]. Unlike ball milling, the slow mixing methods do not reduce particle sizes as no high impact or shear forces are introduced [30]. Owing to various factors such as high surface energy, frictional contacts, elastic interlocking mechanisms and weak attractive forces upon stirring and ultrasonication, the tendency of GNPs to re-agglomerate occurred along with the prolonged powder process time [31]. Therefore, intensive research works have been done to improve the uniformity of dispersion by combining the ball milling and ultrasonication/stirring [32, 33]. In this complex technique, the GNPs de-agglomerating via ultrasonication/stirring should be prior to mixing by conventional ball milling or high-energy ball milling. The choice of this sequence implies the reasons that slow mixing firstly can effectively relieve GNPs agglomeration without exposing them to impact with the hard ceramic particles that can significantly damage the GNPs simultaneously, and the sonication media may become a source of contamination that can adversely affect sintering and full densification when the colloidal process is the last step in the preparation of GNPs–ceramic mixture powder. Nieto et al. [34] uniformly incorporated high volume fractions (5 vol%–15 vol%) of GNPs into Al_2O_3 matrix by utilizing both ultrasonication and ball milling. Porwal et al. [35] have prepared GNPs–Al_2O_3 CMCs with liquid-phase exfoliation of graphene at first and then dispersed them dropwise into Al_2O_3 matrix via ultrasonication and ball milling, resulting in a 40% increment in fracture toughness with only 0.8 vol% addition. This processing route not only solves the problem of producing high-quality graphene without affecting its properties but also produces homogenously dispersed GNPs–ceramic powder with improved properties of CMCs.

2.2 Colloidal processing

Another well-known route to mix graphene with ceramic matrix is colloidal processing, which can be realized via surface modification as direct functionalization (i.e., oxidation) or using surfactants that generate electric charges, facilitating the homogenous dispersion of graphene throughout the ceramic matrix powder as stabilizing suspensions, reducing repulsion, etc. [36, 37]. Stability of graphene in the ceramic suspension is based on the net balance of two predominant forces as electrostatic repulsion and van der Waals forces, and the latter promote agglomeration. In particular, the high negative wall surface potential of graphene is capable of overwhelming van der Waals attractions in distilled water. The improvement of surface potential and electrostatic repulsion can be obtained by adding surfactants (ionic charges), which counterbalances van der Waals attraction and stabilizes the dispersion of graphene. Polyethylene glycol (PEG), 1-methyl-2-pyrrolidone (NMP), 3-aminopropyltriethoxysilane and sodium dodecyl sulfate have been reported as surfactants to stabilize the suspensions [38, 39]. Furthermore, a similar colloidal processing named hetero-coagulation is developed by Wang et al. [40]. In their work,

graphene oxide (GO) and alumina suspension were prepared by ultrasonication in water separately. Owing to electrostatic repulsion and intramolecular dehydration at the edge of GO, meanwhile, alumina particles possessed a surface potential of 32 mV; both of the precursor solutions were well dispersed. Then, GO was added dropwise into the alumina suspension under mild magnetic stirring to obtain a homogeneous distribution of graphene nanosheets in an alumina matrix. The illustration scheme of preparing graphene–metal oxides ceramic composite via hetero-aggregation is shown in Fig. 2 [41]. Centeno et al. [42] demonstrated a similar technique to prepare graphene–alumina-based ceramic composites powder by adding GO dropwise into alumina suspension under mechanical stirring, and the pH value was maintained at 10. Walker et al. [43] have successfully prepared well-dispersed graphene–Si_3N_4 composites via colloidal processing route. A cationic surfactant (cetyltrimethylammonium bromide, CTAB) was used to produce positive charges on both ceramic and graphene surfaces and develop electrostatic repulsive forces on these surfaces. Ascribing to the attraction of hydrophobic graphene to hydrophobic tails of the surfactant, the good dispersion of graphene within the ceramic matrix was successfully guaranteed. Although various colloidal processing routes have been studied, there is still a lack of quantitative information on GNPs and ceramic matrix to accurately compare the dispersion potential and evaluate the dispersion homogeneity of each route in terms of agglomerate size in solutions.

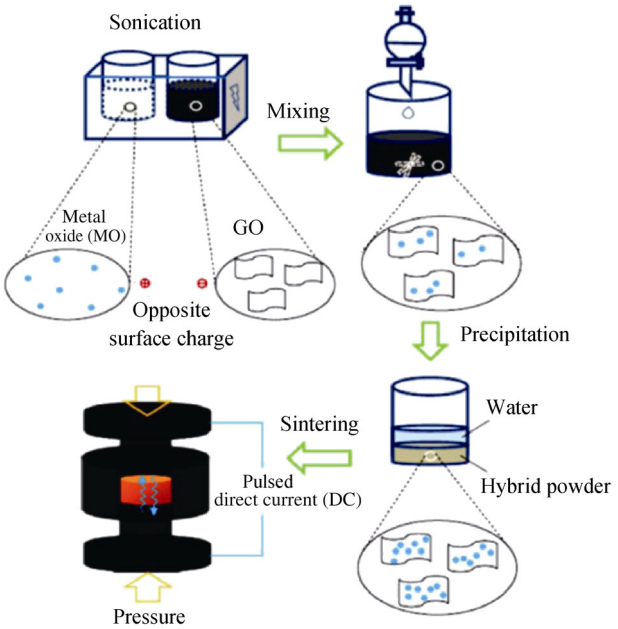

Fig. 2 Illustration of preparing graphene–metal oxides ceramic composite via hetero-aggregation [41]

Specially to GNPs–oxide CMCs, sol–gel processing route has been adopted to disperse GNPs in ceramic composites, mainly for GNPs–silica CMCs. In this method, graphene was firstly dispersed in molecular precursor solution (e.g., tetramethyl orthosilicate, TMOS) and a uniformly dispersed sol was generated by sonicating the suspension of TMOS and graphene. Later, initiated by adding catalyst (e.g., acidic water), hydrolysis was promoted and composite gels was formed upon condensation at room temperature [44]. Mohammad-Rezaei et al. [45] produced a new surface-renewable electrode based on this process with molding and drying. By dispersing into the solution of the sol–gel precursors containing methyltriethoxysilane in methanol and hydrochloric acid, followed by the hydrolysis of methyltriethoxysilane, the GNSs were trapped in the gel. Sol–gel processing provides a good dispersion route by dissolving or suspending materials in liquid phase, which simplifies the preparation of nanosized materials, while the coagulation in precursor suspensions is still a difficult problem that should be tackled.

2.3 Solid-state sintering

As conventional sintering (e.g., pressure-less sintering) requires high temperature and long processing time to fully densify the ceramics, the abnormal grain growth and simultaneous degradation of GNPs in the ceramic matrix seem inevitable. GNPs can be easily oxidized at temperature over 600 °C, which affected the mechanical properties, especially the hardness of the material [46]. Moreover, nanoscaled GNPs may inhibit densification and further increase the sintering temperature required for complete densification of ceramic composites; nevertheless, the high temperature may induce the reactions between graphene and ceramic matrix [47]. Therefore, novel sintering techniques are continuously being exploited with the aim of lowering sintering temperature and shortening dwelling time to overcome the mentioned limitations. For example, hot pressing (HP) and hot isostatic pressing (HIP) have focused on sintering ceramics at lower temperatures by applying pressure, whereas spark plasma sintering (SPS) and microwave sintering focus on sintering ceramics at both lower temperature and shorter dwell time by applying both pressure and electric field to obtain high heating rates [48]. Owing to the simultaneous application of pressure and electric current for the densification of ceramics via creep mechanism, SPS is considered as the dominant powder consolidation technique to create fully dense ceramics, and almost 90% GNPs–CMCs are prepared by this technique recently. The advantages of SPS are concluded as follows [49, 50]. Firstly, the heating rate of SPS is relatively high, which not only improves the sintering efficiency, but also inhibits the grain growth and therefore

avoids the degradation and destruction of graphene. Secondly, as a kind of hot pressing sintering, the maximum pressure imposed by SPS technique can reach 1 GPa, which can effectively improve the density of ceramic composites and reduce the sintering temperature to maintain mechanical properties of graphene and CMCs. Lastly, SPS involves advantages of the in situ reduction of GO to graphene in a single step without requiring any additional steps, and the alignment of graphene occurs in a direction perpendicular to applied pressure. GNPs-reinforced Si_3N_4 CMCs, with 3 wt% and 5 wt% GNPs, were synthesized by SPS [51]. A 100% increase in the fracture toughness was achieved by employing 3 wt% thinner few-layer GNPs as filler material, compared to the monolithic Si_3N_4 samples. The enhanced mechanical properties were attributed to the higher aspect ratio of thinner few-layer GNPs, fast heating rate and uniaxial pressure of SPS, leading to a more homogeneous dispersion, higher interface area and smaller pores in the ceramic matrix. Liu et al. [52] have used SPS to fabricate graphene platelets (GPLs)-reinforced yttria-stabilized zirconia (YSZ) composites, and they are nearly fully consolidated and homogeneously dispersed with GPLs. The addition of GPLs significantly refines structural integrity of the ceramic matrix and makes phase transformation of YSZ from the tetragonal to monoclinic with the presence of GPLs during the high-temperature processing. Around 7% and 60% improvement in hardness and toughness were achieved, respectively, with the addition of GPLs. An interesting work reported by Lahiri et al. [53] showing the shorter CNTs can be unzipped into multilayered graphene sheets within TaC ceramic grains upon SPS. As the two-dimensional GPLs offer higher resistance to pullout, higher transverse rupture strength and delayed fracture could be realized, whereas long CNTs retain the tubular structure. Tapaszto et al. [54] compared the mechanical properties of graphene-reinforced Si_3N_4 composites prepared by different methods. It is shown that by using SPS method, a 10%–20% enhancement and a 30%–40% significant improvement on elastic modulus and hardness values in the composites were realized, respectively, compared with those by HIP method. In contrast, the fracture toughness displayed higher values in the latter case. They emphasized this phenomenon to the different sintering kinetics on the phase transformation of the silicon nitride matrix. For example, the original α-Si_3N_4 grains were mainly transformed to β-Si_3N_4 grains in the HIP sintered composites due to the higher sintering temperature with longer holding time than SPS process, whereas the SPS sintered samples predominantly retained α-Si_3N_4 phase. In addition, the excellent mechanical properties of graphene were expected to be better preserved with SPS method because of the short holding time. They are usually easily damaged during long exposures to high temperatures and decayed substantially.

Referring the particularity of carbon composition in SiC-based ceramics and the research progress in the growth of epitaxial graphene (EG) by the thermal decomposition of SiC [55–58], Miranzo et al. [59] developed graphene-reinforced CMCs via the in situ growth of graphene on SiC. Approximately 4 vol% EG was grown on SiC during SPS process with a few layers of epitaxial graphene found between the grain boundaries of bulk SiC. It provided a single-step route for processing GNPs–CMCs with excellent uniformity of the graphene phase in the ceramic matrix. These composites exhibited an electrical conductivity of 1.02×10^2 $S{\cdot}m^{-1}$ and an enhancement in toughness of 55%. This method provided a possibility for rapid preparation of graphene–SiC composites with excellent electrical conductivity and mechanical properties. However, the continuous network of graphene layers formed between grain boundaries may adversely affect the strength of materials at room temperature.

Currently, high-frequency induction heat sintering (HFIHS) is raised to sinter ceramics over very short sintering time (< 2 min) through the simultaneous application of induced current and high pressure. Kwon et al. [60] demonstrated that graphene–ZrO_2 CMCs can be densified via this technique and the relative density can be as high as 96%. Furthermore, graphene–Al_2O_3 CMCs with near-theoretical densities ($\sim$ 99%) were fabricated by Ahmad et al. [61], adopting HFIHS in processing conditions of 1500 °C, 60 MPa and 3 min. Inspired by this work, it may be possible to enhance the relative density values to near 100% by carefully modifying or optimizing process parameters, for example, increasing the heating rates. Challenges remain to overcome the degradation and agglomeration of the graphene within the ceramic composite, as well as to find a cost-effective way to produce composites with high density.

3 Mechanical properties

3.1 Oxide composites

The introduction of graphene has an obvious effect on the microstructure of ceramic composites, especially on the grain size refinement of ceramic matrix [62]. Taking alumina ceramics for example, the particle size of GNPs–alumina CMCs with 0.6 vol% contents sintered at 1300 °C by SPS is 0.4 μm, which is significantly smaller than that of single-phase alumina ceramics sintered under the same condition (3.1 μm). When increasing the content of graphene to 1.2 vol%, the particle size of ceramic matrix decreases to only 0.3 μm, revealing obvious grain size

refinement attributed to the large specific surface area and the wrapping/anchoring of graphene around ceramic grains, as shown in Fig. 3. As discussed above, a crack to propagate through the graphene rarely appears in the presence of strong bonding between graphene and the ceramic matrix, because it is difficult for the crack to propagate with the high strength and wrapping of graphene around ceramic grains. Moreover, crack bridging was proposed due to graphene pullout and improved the toughness of graphene-reinforced CMCs. Also, the relatively large size of graphene provided a lengthy deflection path that was beneficial to the load transfer. These properties shown in Fig. 4 contribute to the fracture toughness of graphene-reinforced CMCs and make graphene a good reinforcement [63]. Liu et al. [64] have carried out a series of works about incorporating GNPs into an alumina matrix, all of which displayed superior toughness and flexure strength than pure alumina. When the addition of GNPs was 0.38 vol%, the flexural strength and fracture toughness of the GNPs-reinforced CMCs were enhanced by 30.75% and 27.20%, respectively, reaching (523 ± 30) MPa and (4.49 ± 0.33) MPa·$m^{1/2}$. However, the agglomeration of GNPs was indicated by the scanning electron microscopy (SEM) images of fracture surfaces showing thick platelets (∼>110 nm) when the GNPs content further increased. As these thick platelets were not flexible, a decline in wrapping of graphene around ceramic grains happened. More

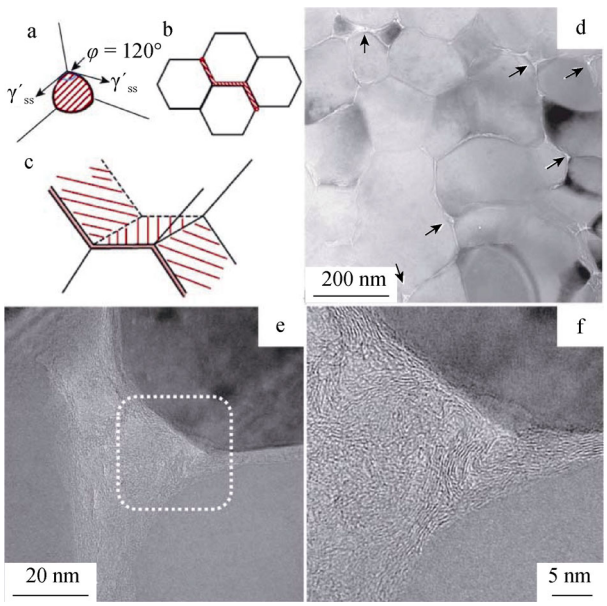

Fig. 3 Schematic illustration showing 2D graphene retarding coarsening of grain most effectively: **a** situation of nanoparticle, **b** 1D inclusion and **c** 2D inclusion [62]; **d** TEM image of 2D few-layer graphene (FLG) platelets-constructed 3D network (arrows indicate triple junctions where FLG platelets are highly wrinkled); **e** TEM image of a typical triple junction containing highly wrinkled FLG and **f** magnified image of white square area in **e** [66]

pores were likely to form between agglomerated GPLs and ceramic matrix interface, inducing localized porosity and hence causing lower densification. The presence of these pores inevitably reduced the contact area of ceramic matrix with GPLs and served as crack initiation sites upon indentation load, hindering the ability of GNPs to reinforce the matrix. In conclusion, mechanical properties of graphene-reinforced CMCs do not show proportional improvement with graphene content increasing in almost all studies [48]. Following this work, the same research group reported a study on alumina-based CMCs with dual reinforcements of GPLs and silicon carbide (SiC) nanoparticles. Compared with pure alumina ceramic, the CMCs showed approximately 36%, 40% and 50% increase in hardness, flexural strength and fracture toughness, respectively, due to more uniform distribution and greater grain size refinement than alumina matrix with sole filler [65]. In contrast, a 50% improvement on the mechanical properties of the alumina and an increase in the electrical conductivity up to eight orders of magnitude with a very low graphene loading (0.22 wt%) were reported by Centeno et al. [42] due to the crack bridging phenomena. Fan et al. [66] observed a ∼40% increase in the strain tolerance of GNPs–Al_2O_3 CMCs with 2.18 vol% GNPs due to the decreased stiffness and increased toughness induced by GNP crack bridging and kinking mechanisms shown in Fig. 3d–e. Since graphene is a very good lubricant by itself because of its hexagonal structure, plenty of research work has been carried out on the friction and tribological properties of graphene-reinforced CMCs. Kim et al. [67] presented a decline from 0.637 to 0.449 in friction coefficient of GNPs-reinforced alumina CMCs with an addition of 1 vol% graphene under the load of 25 N, along with a decrease from 2.12×10^{-4} to 2.18×10^{-5} $mm^3 \cdot N^{-1} \cdot m^{-1}$ in wear rate. Therefore, graphene can significantly improve tribological properties of CMCs. Furthermore, Yazdani et al. [38] measured the tribological performance of graphene–CNTs-hybrid-reinforced Al_2O_3 CMCs by using ball-on-disk method. Compared with the wear rate and friction coefficient of monolithic Al_2O_3 ceramic, those of Al_2O_3 CMCs containing (0.5 wt% GNPs, 1.0 wt% CNTs) and (0.3 wt% GNPs, 1.1 wt% CNTs) showed remarkable 70% and 80% reduction, 23% and 20% decrease, respectively, under the load of 15 N. In this hybrid system, GNPs played a vital role in the formation of tribofilm on worn surface by exfoliation, whereas CNTs prevented grain from being pulled out during the tribological test and helped to improve the fracture toughness. The excellent coordination between GNPs and CNTs significantly promoted the wear resistance properties of the CMCs.

It is without doubt that the quality of graphene plays a crucial role in determining the mechanical properties of the CMCs. Compared with GNPs reduced from GO possessing

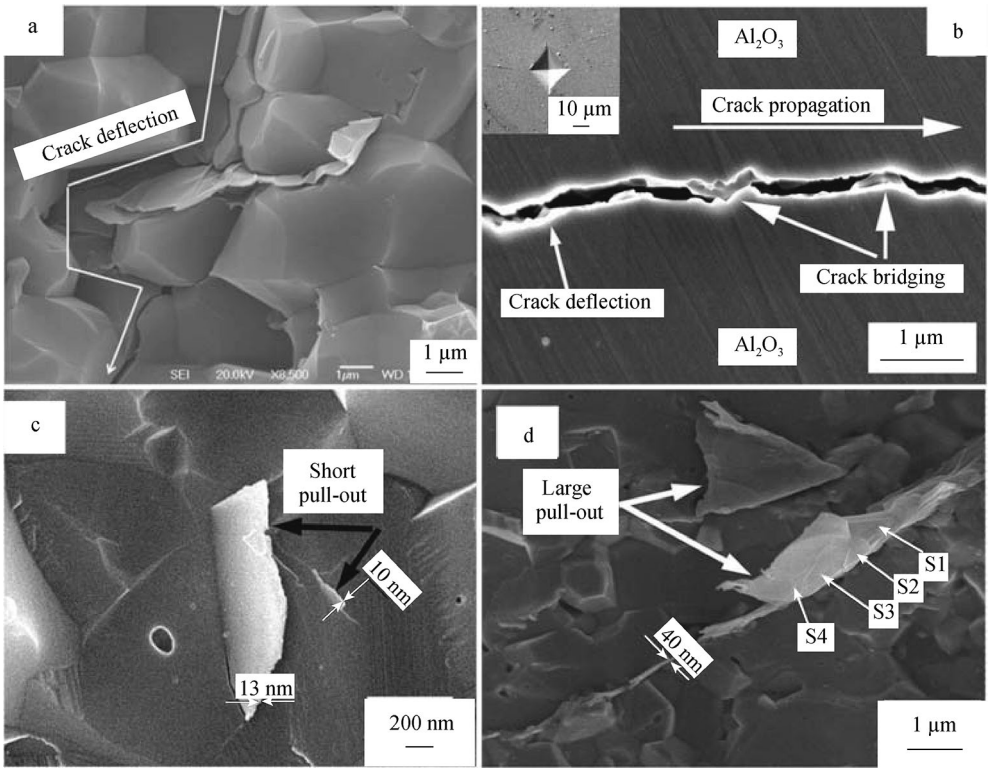

Fig. 4 SEM images for GNPs-induced toughening mechanisms in Al_2O_3 ceramic matrix: **a** crack deflection [64], **b** crack deflection and bridging, **c** short GNPs pullout segment and its adhesion with Al_2O_3 matrix, and **d** relatively larger-sized GNPs pullout areas exhibiting discrete graphene layers (small white arrows) [61]

a lot of defects, the defect-free graphene obtained by mechanical exfoliation method is more conducive to improve the flexural strength and other mechanical properties of CMCs. The mechanical properties of Al_2O_3 CMCs reinforced with un-oxidized graphene, GO and reduced GO were compared by Kim et al. [67], and un-oxidized graphene–alumina composites exhibited the best results, suggesting an improvement of ~ 48%, ~ 28% and ~ 95% in fracture toughness, flexural strength and wear resistance, respectively, due to the less defect concentration. In addition, they also investigated the effects of graphene size (~ 100, 20, and 10 μm, respectively) on fracture toughness of graphene–alumina CMCs. Owing to structural defects produced by graphene flakes of ~ 100 μm, the toughening mechanisms such as crack bridging were less dominant when smaller flakes (~ 10 μm) were used. The best results were obtained when the lateral size of graphene flakes is ~ 20 μm. Although an increase in flexural strength of alumina CMCs reinforced by non-oxidized GNS was generally observed, it is worth noting that better interfacial bonding can be obtained when using graphene with carbides (e.g., B_4C, SiC) and GO with oxides (e.g., Al_2O_3, ZrO_2) to improve the mechanical properties [68, 69].

Recently, various works have been carried out by adopting hybrid nanocarbon materials and complex oxide ceramic matrix to enhance the mechanical properties of CMCs. Yazdani et al. [38] prepared Al_2O_3 CMCs reinforced with hybrid nanocarbon materials (GNPs and CNTs) via a combination of wet dispersion technique and hot pressing. The average fracture toughness of the CMCs was improved from 3.5 to 5.7 MPa·$m^{1/2}$ with an increment in flexural strength from 360 to 424 MPa, and the hybrid additions are 0.5 wt% GNPs and 1 wt% CNTs. The increased values in toughening properties are attributed to the attachment of CNTs to the surfaces and edges of GNPs during the mixing process, which assisted de-agglomeration and homogenous dispersion within the matrix. Later, Ahmad et al. [70] proposed to fabricate alumina-based CMCs with high performance of densification behavior and fracture toughness by using HFIHS process, adopting silicon carbide nanoparticles (SiC NPs) as the second reinforcement. Fractography of the samples revealed a transition from a mixed intergranular/transgranular mode for SiC NPs or GNP-reinforced nanocomposites to transgranular fracture mode for the hybrid nanocomposites. It is because the SiC NPs presented within or at the grain boundary areas, whereas the GNPs anchored between neighboring grains. An improvement of 160% and 27% in

fracture toughness and microhardness can be detected when incorporating as little as 0.5 wt% GNPs along with 5.0 wt% SiC NPs, respectively. The enhancement is mainly attributed to the synergic effects of the nanostructured reinforcements and GNPs, including their distinctly different toughening mechanisms, such as crack deflection and pullout effects of SiC NPs, and interlayer slithering of GNPs. Jiang et al. [71] fabricated GPLs-reinforced zirconia-toughened alumina (ZTA) CMCs using SPS. The fracture toughness of the ZTA CMCs resulted in an increment of a 29% by loading GPLs, which is higher than that of the pure alumina matrix (26.4%). Similar to other graphene ceramic composites, the main toughening mechanisms induced by GPLs are pullout, crack bridging and crack deflection.

3.2 Non-oxide composites

Similar to the toughening mechanisms in GNPs–oxide CMCs, most of the studies on graphene-reinforced non-oxide CMCs have shown toughening mechanisms originated from pullouts, crack deflection, crack branching and crack bridging (Fig. 5). Besides, cracks cannot propagate through graphene walls and were forced to deviate around the graphene sheets due to the wrapping effect of graphene around the grains as a two-dimensional material. Walker et al. [43] observed this touching mechanism and obtained an improvement of 235% in fracture toughness with only 1.5 vol% multilayer graphene content in Si_3N_4 matrix. What is more, graphene plays an important role in the friction and wear behavior of ceramic composites. Llorente et al. [72] investigated the effects of GNPs content and graphene source on the friction performance and showed an enhanced wear resistance of up to $\sim$ 70% for the material containing 20 vol% GNPs compared to monolithic SiC. They ascribed the improved tribological behavior of the GNPs–SiC ceramic composites to the formation of an adhered lubricating and protecting tribofilm according to the analysis of the wear debris by micro-Raman spectroscopy. It is found that multilayered graphene participated more actively in the protecting tribofilm than other graphene sources such as in situ grown graphene and reduced GO. Similarly, Belmonte et al. [73] prepared the GNPs–Si_3N_4 ceramic composites by SPS technology. The ceramic composites possessed excellent friction properties as an improvement of 56% in the wear resistance and a reduction in friction coefficient compared with the Si_3N_4 ceramic matrix, which consequently improved the average service life. Tapasztó et al. [74] further confirmed that a continuous protecting and lubricating tribofilm consisted of FL-GNPs with high structural quality contributing to a remarkable improvement in the tribological properties of

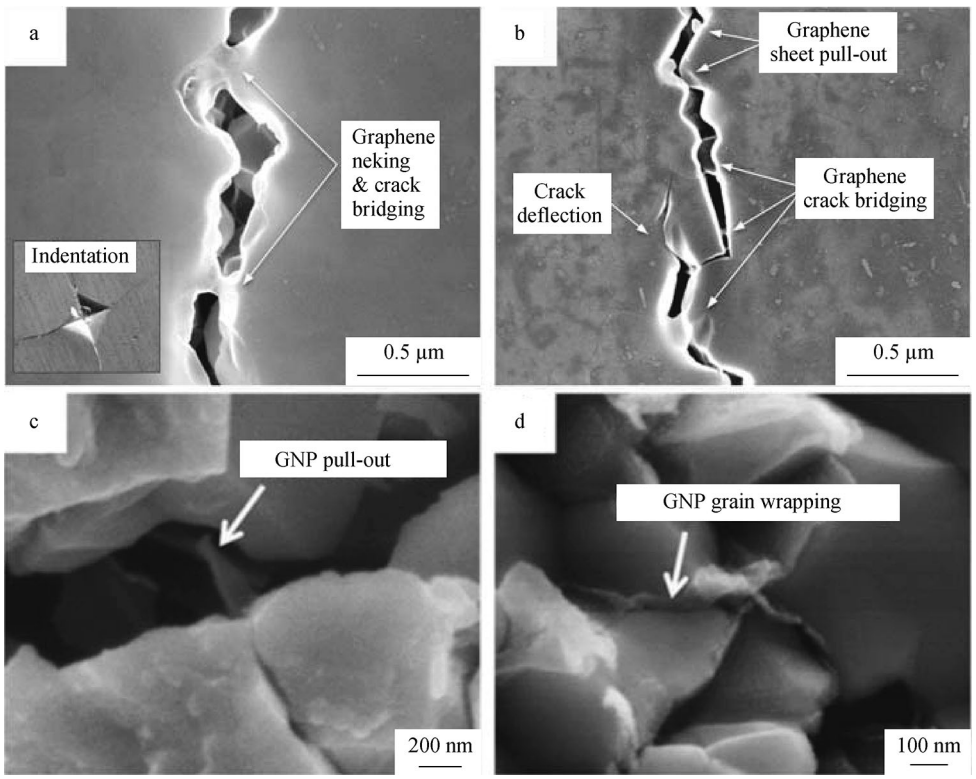

Fig. 5 SEM images for various toughening mechanisms in graphene–Si_3N_4 CMCs [43]: **a** graphene necking and crack bridging, **b** crack deflection, bridging and pullout; and in graphene–TaC CMCs [83]: **c** GNPs pullout, **d** GNPs grain wrapping

GNPs–Si_3N_4 ceramic composites. Compared with monolithic Si_3N_4, only 5 wt% GNPs addition can increase wear resistance by more than 20 times and reduce the friction coefficient by 50%. Meanwhile, the hardness, bending strength and fracture toughness were also improved by the addition of the graphene. Components produced from such materials can greatly reduce the loss during operation and significantly improve their durability in contact mechanical applications, which are expected to be used in gasoline direct injection system.

In addition, Seiner et al. [75] illustrated a significant anisotropy of the Young's elastic modulus and the internal friction in the GNPs–Si_3N_4 ceramic composites with just 3 wt% GNPs, while the anisotropy of the shear modulus was much less severe. The shear internal friction was strongly anisotropic with the maximal value corresponding to the volume-preserving, 'breathing' vibrations of the GNPs. Shearing along the basal planes and in the out-of-plane direction led to the decrease of $\sim$ 15%, while shearing along the platelet thickness showed no significant difference from the Si_3N_4 reference. Internal shear friction of the GNP composite was shown to be significantly higher in the out-of-plane direction. Koller et al. [76] showed that the highly anisotropic elastic behavior and attenuation of GNPs is intrinsic to their structure evaluated by acoustic properties of a bulk GNPs compact. It was observed that elastic coefficients differed by a factor of 20 in the basal and *c*-axis directions. Similar results of anisotropic softening were observed by Rutkowski et al. [77] on Si_3N_4–GNPs composites. GNPs-induced softening was seen to be greater in *c*-axis direction (parallel to the sintering pressure axis). Fracture toughness was lower in the in-plane direction (perpendicular to sintering pressure) than in the out-of-plane direction; however, both were higher than that of the unreinforced material. Tapaszto et al. [78] investigated the distribution of GNPs in Si_3N_4 ceramic matrix prepared by SPS and HIP sintering methods, with uniaxial and isotropic pressures applied, respectively. It is found that more than 80% GNPs lay within $\pm$ 15° deviation from a preferred orientation direction in the SPS sintered samples in Fig. 6, which is perpendicular to the uniaxial pressure direction and in contrast to HIP sintered samples where a closely random orientation is revealed. These results well explained the anisotropic mechanical, electrical and thermal properties of GNPs-reinforced CMCs prepared under uniaxial pressure conditions by several widely used sintering methods.

It should be noted that some conductive ceramics with metallic bonding such as ZrB_2 and TaC present better mechanical and functional properties with increased content of GNPs [79, 80]. SPS processing improved electrical conductivity of GNPs as the current flows through both the powder and the graphite dies, in contrast to non-conductive ceramics such as Al_2O_3. That is why GNPs with high volume fraction did not induce porosity in ZrB_2- and TaC-based composites and exhibited no adverse effects in densification. Yadhukulakrishnan et al. [81] prepared GNPs-reinforced ZrB_2 system ceramics and achieved promising improvements of 83% and 95% in fracture toughness and flexure strength with the addition of 6 vol% GNPs, respectively, along with an increase in relative density from $\sim$ 85% to 97%. Asl et al. [82] observed a significant rise in the level of densification by adding GNPs in the ZrB_2-SiC composites, which has led to an increase in hardness indirectly. The advantages in GNPs-reinforced conductive ceramics composites were also illustrated by Nieto et al. [83] who successfully synthesized the GNPs–TaC composites with enhanced fracture toughness. The densification was enhanced to 99% theoretical density with an addition of 5 vol% GNPs, while the grain sizes were reduced by over 60% through grain wrapping mechanism. Owing to the high electrical and thermal conductivity of GNPs, more uniform heating distribution took place during SPS processing, and thus the densification and fracture toughness were improved simultaneously.

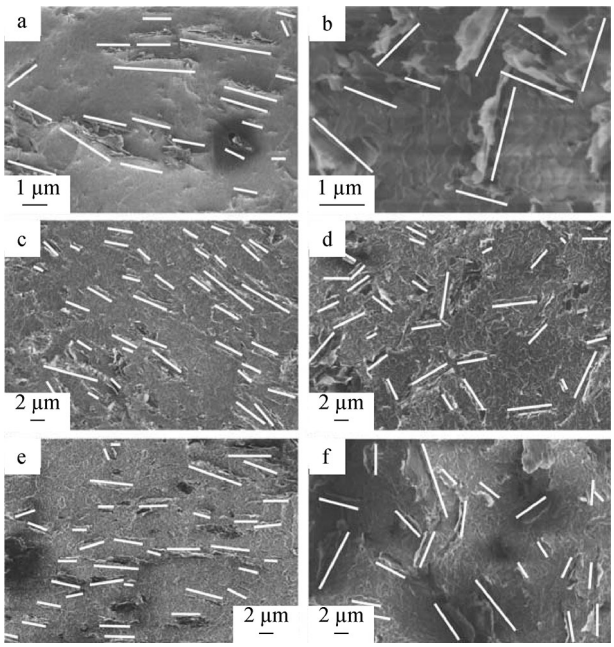

Fig. 6 Fracture surface SEM images of Si_3N_4 composites containing 3 wt% GNPs prepared using **a, c, e** SPS and **b, d, f** HIP sintering methods (position and orientation of GNPs can be clearly identified in micrographs with white lines marking) [78]

4 Functional properties

In addition to mechanical properties, graphene also possesses excellent electrical and thermal conductivity, which

Table 1 Overview of functional properties of GNPs-reinforced CMCs as reported in the literature

Matrix material	Nanofiller type	Nanofiller content	Processing technique	Percolation threshold	Electrical conductivity	Thermal conductivity	Ref.
Al_2O_3	GNPs	0 vol%–15 vol%	Powder/SPS	3 vol%	5709 $S·m^{-1}$ for 15 vol%	NA	[26]
Al_2O_3	GO	2 wt%	Colloidal/SPS	NA	172 $S·m^{-1}$	NA	[40]
Al_2O_3	GO	0.16 wt%, 0.22 wt% and 0.45 wt%	Colloidal/SPS	0.22 wt%	11.1 $S·m^{-1}$ for 0.45 wt%	NA	[42]
Al_2O_3	GNPs	0 vol%–2 vol%	Powder/HP	<0.5 vol%	123.3 $S·m^{-1}$ for 2 vol%	NA	[85]
Al_2O_3	Expanded graphite	0 vol%–9.5 vol%	Powder/HP	4.7 vol%–5.7 vol%	9.6×10^{-2} $S·m^{-1}$ for 9.4 vol%	NA	[86]
Al_2O_3	GO	0 vol%–2.35 vol%	Colloidal/SPS	0.38 vol%	1038.15 $S·m^{-1}$ for 2.35 vol%	NA	[87]
Al_2O_3	GPLs	0 vol%–15 vol%	Powder/SPS	7.1 vol%	20.1 $S·m^{-1}$ for 15 vol%	15 $W·m^{-1}·K^{-1}$ at 600 °C for 15 vol%	[89]
SiO_2	GO	0 wt%–1 wt%	Colloidal/SPS	< 0.58 wt%	0.01 $S·m^{-1}$ for 0.98 wt%	NA	[39]
ZrO_2	GNPs	3 wt%	Powder/HFIHS	< 1 wt%	98 $S·m^{-1}$ for 3 wt%	NA	[60]
MgO	GNSs	0 vol%–7 vol%	Powder/HP	NA	NA	33.9 $W·m^{-1}·K^{-1}$ for 7 vol%	[92]
Si_3N_4	GNPs	4 vol%–25 vol%	Powder + colloidal/SPS	7 vol%–9 vol%	40 $S·m^{-1}$	NA	[94]
Si_3N_4	GNPs	4.3 vol%–24.4 vol%	Powder/SPS	NA	NA	40 $W·m^{-1}·K^{-1}$	[98]
SiC	GNPs	4 vol%	Powder/SPS	NA	102 $S·m^{-1}$ for 4 vol%	NA	[59]
SiC	GNPs	0 vol%–20 vol%	Colloidal/SPS	NA	NA	152 $W·m^{-1}·K^{-1}$ (perpendicular) and 9.9 $W·m^{-1}·K^{-1}$ (parallel) to the SPS axis	[99]
B_4C	GNPs	0 vol%–5 vol%	Powder/HP	< 1 vol%	6500 $S·m^{-1}$ for 5 vol%	48 $W·m^{-1}·K^{-1}$ for 5 vol%	[96]
B_4C	GPLs	4 wt%–10 wt%	Powder/HP	NA	1526 $S·m^{-1}$ (perpendicular), 872 $S·m^{-1}$ (parallel) to the HP axis for 8 wt%	NA	[97]

makes it possible to functionalize structural ceramics. Table 1 summarizes the electrical and thermal properties of GNPs-reinforced CMCs reported in the literature so far.

4.1 Oxide composites

The alumina ceramic is a typical insulator with electrical conductivity of only 1×10^{-13} $S·m^{-1}$ at room temperature. When introducing a conductive material into the insulator ceramic matrix, the composite material changes from insulation to conductivity at a critical volume fraction value of the conductive phase. This phenomenon is called percolation, and the sudden change point is named percolation threshold. One of the earliest studies on percolation threshold for graphene-reinforced CMCs was carried out by Fan et al. in year 2010 [26]. They fabricated alumina-based CMCs with 0 vol%–15 vol% graphene loading by SPS and demonstrated that the percolation threshold for the ceramic composite was around 3 vol%. The improvement in electrical conductivity was particularly significant beyond the percolation threshold and reached a value of 5709 $S·m^{-1}$ with the addition of 15 vol% graphene. It was higher than that of any CMCs reinforced with the same volume fraction of CNTs. The enhanced electrical conductivity was attributed to an efficient network formed by the overlapping GNPs, and it increased the number of charge carriers across the composites. Owing to the high aspect ratio and high surface area of GNPs, superior contact can be provided in contrast to CNTs where point-to-point contact occurs and may induce higher resistance.

Thus, the onset of percolation threshold may decrease with an increasing aspect ratio (L/D) of graphene with uniformly dispersed particles [84–86]. In a later study by Fan et al. [87], colloidal processing was adopted to prepare well-dispersed GO and alumina composite powders, where GO was reduced to graphene via SPS processing. The percolation threshold was successfully decreased to 0.38 vol%, which is much lower than the previously reported value of 3.0 vol%. The good results can be explained by the good dispersion and high quality of graphene used and the multidimensional electron transport pathways. The electrical conductivity was 1×10^3 S·m^{-1} for only 2.35 vol% loading of graphene. Furthermore, the percolation threshold was further reduced to 0.22 wt% in the work of Centeno et al. [42]. Conductivity was improved up to eight orders of magnitude compared to unreinforced alumina.

More interestingly, the Hall coefficient reversed its sign from positive to negative with more grapheme added, revealing a change in the major charge carrier, as ascertained by the change of positive to negative in Seebeck coefficient. It is inferred that the positive Hall coefficients with low graphene content are induced by the doping effect of alumina matrix. Owing to the mismatch in coefficient of thermal expansion, the graphene would firmly wrap the alumina ceramic particle and generate high pressure during cooling when the graphene loading is low. Therefore, in an environment with low oxygen partial pressure at high temperature, oxygen vacancies and aluminum interstitials provided positive defects acting as electron acceptor, and graphene doped with holes accordingly, presenting a positive value of Hall coefficient. With the increase in graphene content, the average thickness of graphene rose due to the overlap between layers. It effectively reduced the possibility of contact between graphene and ceramic matrix and manifested the intrinsic charge carrier type of graphene that should be electrons as they were chemically reduced. What is more, Fan et al. [87] also tailored the charge carrier type by varying the matrix from Al_2O_3 to Al_2O_3-3YSZ and Al_2O_3-8YSZ. As pure GO and Al_2O_3 samples had negative Seebeck coefficient and appeared with n-type carrier doping, increased YSZ content yielded higher Seebeck coefficient due to the alteration of the surface state with the increased oxygen concentration. The change of positive to negative is unique and has not been reported in other composites. These tunable carrier-type graphene–Al_2O_3 CMCs are considered as promising new materials, especially in the harsh environment (radiation, high temperature, corrosion resistance, etc.).

Except the effect on enhanced electrical conductivity, the addition of graphene in oxide CMCs also promoted their thermal properties. Rutkowski et al. [88] have directly measured a series of thermal properties of GNPs–Al_2O_3 composites prepared by both HP and SPS with up to $\sim$ 16.5 vol% GNPs, including thermal stability, thermal diffusivity, specific heat and thermal conductivity. Thermal gravimetric analysis conducted under ambient conditions was adopted to explain the thermal stability of GNPs–Al_2O_3 composites. It is concluded that the composites could bear the temperature up to 1000 °C with GNPs content < 3.5 vol%, whereas the composites began to experience oxidation at temperatures of 550–700 °C with higher volume fractions of GNPs. Thermal diffusivity presented an anisotropy of up to 89% in composites with 16.5 vol% GNPs. It is because an increased diffusivity along the pressing axis was shown with the increased GNP contents, while the thermal diffusivity in the direction perpendicular to the pressing axis stayed the same and increased slightly at higher volume fractions for HP samples. A reduction in thermal conductivity calculated in most samples was inferred to the lower densification induced by GNPs and the introduction of low-conductivity zirconia during ball milling of powders. Only when the GNP content exceeded 10 vol%, the thermal conductivity was enhanced by GNPs in HP samples because of the higher orientation of GNPs achieved. The anisotropic thermal properties are also reported by Celik et al. [89] in GPLs–Al_2O_3 composites prepared by SPS. Oriented GPLs led to a less resistive heat conduction path in the in-plane direction; therefore, $\sim$ 44% increase in the in-plane thermal conductivity was achieved at 600 °C with 15 vol% GPLs addition and $\sim$52% increase in the in-plane-to-through-thickness thermal conductivity ratio ($k_{\text{in-plane}}/k_{\text{through-thickness}}$).

Furthermore, according to the equation for calculating thermoelectric figure of merit $zT = (\sigma S^2/k)T$, where σ, S, k and T are the electrical conductivity, Seebeck coefficient, thermal conductivity and absolute temperature, respectively, it is an effective strategy to increase thermoelectric efficiency by reducing the lattice thermal conductivity by grain boundary engineering and without deterioration of electron transport [90]. Although the thermal conductivity of graphene is extremely high, the addition of graphene produces lower thermal conductivity due to the lower density and smaller grain size after sintering. Lin et al. [91] speculated that graphene sheets may act as thermal barrier when they lay on the plane perpendicular to the heat conduction according to the unique anisotropic thermal characteristics, therefore blocking the movement of phonons when they are interconnected. Moreover, as phonon transportation is sensitive to the presence of lattice defects, large plenty of defects introduced from the external heat and load used during SPS may further reduce the thermal conductivity. Chen et al. [92] prepared highly dense GNSs–magnesia composites by hot pressing, and they evaluated the effect of GNSs content (0 vol%–7 vol%) on microstructural, mechanical and thermal properties. Based

on the previous results that incorporating GNSs may inhibit the sintering and grain growth of MgO, a significant decrease in thermal conductivity could be detected from 55.8 $W{\cdot}m^{-1}{\cdot}K^{-1}$ for MgO to 33.9 $W{\cdot}m^{-1}{\cdot}K^{-1}$ for 7 vol% GNSs–MgO along the hot-pressing direction. Besides, the thermal conductivity of monolithic MgO and 2 vol% GNSs–MgO composite at elevated temperatures was also investigated, showing a remarkable decrease first and then plateau beyond 700 °C. This decrease can be easily attributed to the coefficient mismatch in thermal expansion, showing enhanced phonon scattering and interface separation.

4.2 Non-oxide composites

Ramirez et al. [93] prepared GNPs–Si_3N_4 CMCs containing 12 wt% and 15 wt% GNPs and systematically investigated the influence of GNPs contents in electrical conductivity and the anisotropic electrical responses. Attributing to the excellent conductivity of graphene and the improved inter-GNPs contacts with the increased GNPs content, the effective current per conducting pixel of the 15 wt% GNPs composites was four times larger than that of the 12 wt% composite. Although the intrinsic electrical anisotropy of graphene sheets presented much higher conductivity in *a*–*b* plane than in *c*-axis direction, the calculated effective current for the perpendicular surface was twice more than that for the parallel orientation. As simply illustrated in Fig. 7, the lateral GNP–GNP junctions provided an additional hopping resistance for charge transport and enhanced scattering at the interplatelet junctions for the parallel geometry. It is noteworthy that an amorphous reaction layer was observed between the GNPs–Si_3N_4 interfaces, which was expected to act as an insulator and may have adverse effects on the transfer of electrons, especially in the direction aligned with the GNPs basal plane. To conclude, unbalanced weight and nature of the resistors forming the percolated network were developed to explain these results. The same research group [94] further increased the graphene content to improve the electrical conductivity of the Si_3N_4-based CMCs. They reported electrical conductivity of 40 $S{\cdot}cm^{-1}$ with a GNPs loading of up to 20 vol% and confirmed the preferential orientation of GNPs in the ceramic matrix. Moreover, electrical conductivity values perpendicular to the pressing axis (aligned with the GNPs basal plane) were found to be an order of magnitude higher than those parallel to the pressing direction in the fixed GNPs content composite, according to the preferred alignment of GNPs during SPS processing. They also reported a percolation threshold of 7 vol%–9 vol%, and different mechanisms of charge transport depended on the conductivity measuring direction. A variable range hopping mechanism dominated charge transport in the perpendicular direction to the pressing axis, while in the parallel direction, the conduction mechanism was more complicated as a metallic transition ($dr/dT < 0$) at higher volume fractions (> 17 vol%) of GNPs was presented.

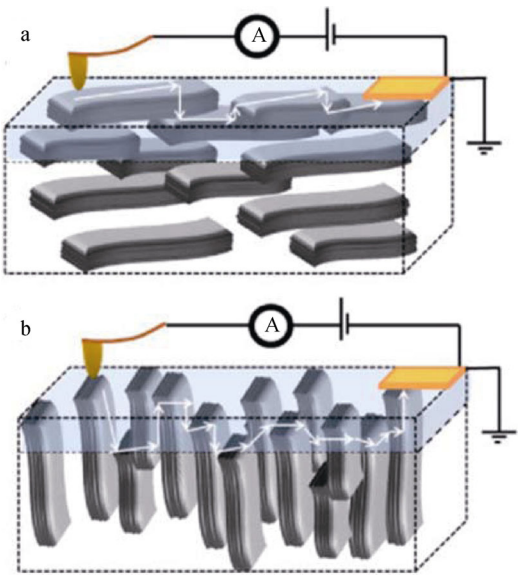

Fig. 7 Simplified schematics of possible conducting paths for orientations **a** perpendicular and **b** parallel to SPS pressing axis [93]

The anisotropic electrical behavior was also detected in the GNPs–SiC CMCs prepared by Roman-Manso et al. [95], as a result of preferential orientation of the GNPs perpendicular to the pressing axis under the applied pressure (50 MPa) during SPS. The electrical conductivity values in the direction perpendicular to the pressing axis were 4–6 times higher than the parallel counterparts. In addition, the electrical conductivity could reach 4380 $S{\cdot}m^{-1}$ at room temperature with 20 vol% GNPs addition, which was three orders of magnitude higher than those without GNPs. Tan et al. [96] well established an electrical percolating network in B_4C CMCs with an incorporation of GNPs as low as 1 vol%, and the electrical conductivity was enhanced correspondingly to 250 $S{\cdot}m^{-1}$. It is almost 10 times higher than that of original B_4C ceramic. Such low percolation threshold could be attributed to the uniform distribution and high aspect ratio of GNPs as well as the crack bridging conducted by TiB_2 particles produced from reactions between B_4C and Ti_3AlC_2. Remarkably, this electrical level was sufficient for electrical discharge machining fabricated from B_4C CMCs after processing test. Similarly, the thermal conductivity of GNPs–B_4C composites presented high anisotropy with significantly enhanced values perpendicular to the hot-pressing axis, while slightly suppressed values were observed in parallel direction. A maximum thermal conductivity of 48 $W{\cdot}m^{-1}{\cdot}K^{-1}$ was obtained in the direction perpendicular

to the pressing axis in B_4C composite with 5 vol% GNPs addition. Based on these results, Sedlak et al. [97] increased GPLs addition of up to 8 wt% in the GPLs–B_4C CMCs prepared by hot pressing at 2100 °C in argon and obtained the electrical conductivity of 1526 $S{\cdot}m^{-1}$ in the perpendicular and 872 $S{\cdot}m^{-1}$ in the parallel direction to the hot-pressing axis, respectively.

Miranzo et al. [98] reported an anisotropic thermal response in GPLs–Si_3N_4 CMCs, presenting an increased thermal conductivity perpendicular to the pressing axis, whereas that value in parallel direction decreased. The thermal conductivity in the direction perpendicular to the pressing axis especially increased twice compared with that of the pure Si_3N_4 matrix. This phenomenon was attributed to the preferential orientation of GPLs in the ceramic matrix under SPS pressing, which formed a more conductive network in the in-plane direction and thus undoubtedly increased the thermal conductivity. A noticeable anisotropic thermal conductivity appeared in the study of Roman-Manso et al. [99] as well, where the room temperature thermal conductivity (K_T) values were 1.5–3.4 times higher in the perpendicular direction than in the parallel direction to the SPS pressing axis, according to the major orientation of GNPs in reinforced SiC CMCs. The reduction in cross-plane thermal conductivity was ascribed to the much lower intrinsic conductivity of the added GNPs in the *c*-axis as the estimated K_T values of the GNPs in the basal plane and along the *c*-axis are 152 and 9.9 $W{\cdot}m^{-1}{\cdot}K^{-1}$, respectively. However, the trend of thermal conduction in GNPs-reinforced high thermal conductor ceramic as AlN is contrary to that stated for other GNPs-reinforced CMCs. Sharp decreases in thermal conductivity for both directions were observed in GNPs–AlN CMCs [100] due to the thermal contact resistance ascribed to a strong coupling at the AlN–graphene interface. Additionally, these GNPs–AlN CMCs developed a high electrical conductivity when the GNPs content was larger than 5 vol%, therefore producing useful materials for applications in the fields such as light-emitting diodes or microelectromechanical systems.

5 Conclusions and outlook

This paper systematically summarizes the related research and reports of GNPs-reinforced CMCs based on the different ceramic matrices. The effects of processing methods and microstructures on mechanical and functional properties of the composites are comprehensively discussed. It can be concluded that: (1) the introduction of GNPs as reinforcements can effectively improve the mechanical properties of CMC materials such as strength, fracture toughness and strain tolerance, relying on the toughening mechanisms as pullout, crack bridging and crack deflection; (2) in respect of functional properties, GNPs-reinforced CMCs possess low percolation threshold and excellent electrical conductivity. The thermal conductivity can be tuned by selecting the GNPs content and ceramic type. Therefore, the combination of enhanced mechanical properties along with improvements in functional properties makes GNPs-reinforced CMCs exciting and promising candidates to promote the advances of technologies.

However, even though large amount of work has been carried out to have an in-depth understanding of graphene roles and their reinforcing mechanisms in ceramics, there remain many challenges that should be solved to fully utilize the potential of these composites. They are included but not limited to the following: (1) more types of ceramic matrices, especially some thermoelectric ceramics, needed to be investigated by endowing better mechanical and thermoelectric properties from GNPs; (2) in order to improve the performance of GNPs-reinforced CMCs, more advanced processing techniques should be explored. We should not only further improve the quality of graphene on the premise of guaranteeing large-scale preparation, but also adopt more effective means to homogeneously disperse GNPs into ceramic matrices with ordered arrangement.

Acknowledgements This study was financially supported by the National Natural Science Foundation of China (Nos. 51432004 and 51672041), the Fundamental Research Funds for the Central Universities (No. 2232018G-07), the Innovation Program of Shanghai Municipal Education Commission (No. 2017-01-07-00-03-E00025), the Program for Innovative Research Team in University of Ministry of Education of China (No. IRT_16R13) and Shanghai Sailing Program (No. 17YF1400400).

References

[1] Centeno A, Rocha VG, Alonso B, Fernandez A, Gutierrez-Gonzalez CF, Torrecillas R, Zurutuza A. Graphene for tough and electroconductive alumina ceramics. J Eur Ceram Soc. 2013;33(15–16):3201.
[2] Yazdani B, Xia YD, Ahmad I, Zhu YQ. Graphene and carbon nanotube (GNT)-reinforced alumina nanocomposites. J Eur Ceram Soc. 2015;35(1):179.
[3] Markandan K, Tan MTT, Chin J, Lim SS. A novel synthesis route and mechanical properties of Si–O–C cured Yytria stabilised zirconia (YSZ)-graphene composite. Ceram Int. 2015; 41(3):3518.
[4] Sternitzke M. Structural ceramic nanocomposites. J Eur Ceram Soc. 1997;17(9):1061.
[5] Niihara K. New design concept of structural ceramics-ceramic nanocomposites. J Ceram Soc Jpn. 1991;99(10):974.
[6] Cho J, Boccaccini AR, Shaffer MSP. Ceramic matrix composites containing carbon nanotubes. J Mater Sci. 2009;44(8): 1934.
[7] He B, Li Y, Zhang HY, Wu DL, Liang LH, Wei H. Phase transformation of ZrO_2 doped with CeO_2. Rare Met. 2018; 37(1):66.

[8] Novoselov KS, Geim AK, Morozov SV, Jiang D, Zhang Y, Dubonos SV, Grigorieva IV, Firsov AA. Electric field effect in atomically thin carbon films. Science. 2004;306(5696):666.
[9] Weitz RT, Yacoby A. Nanomaterials: graphene rests easy. Nat Nanotechnol. 2010;5(10):699.
[10] Lee C, Wei XD, Kysar JW, Hone J. Measurement of the elastic properties and intrinsic strength of monolayer grapheme. Science. 2008;321(5887):385.
[11] Geim AK. Graphene: status and prospects. Science. 2009; 324(5934):1530.
[12] Van BJ. Graphene: from strength to strength. Nat Nanotechnol. 2007;2(4):199.
[13] Nair RR, Blake P, Grigorenko AN, Novoselov KS, Booth TJ, Stauber T, Peres NMR, Geim AK. Fine structure constant defines visual transparency of graphene. Science. 2008; 320(5881):1308.
[14] Huang X, Yin ZY, Wu SX, Qi XY, He QY, Zhang QC, Yan QY, Boey F, Zhang H. Graphene-based materials: synthesis, characterization, properties, and applications. Small. 2011; 7(14):1876.
[15] Edwards RS, Coleman KS. Graphene synthesis: relationship to applications. Nanoscale. 2013;5(1):38.
[16] Singh V, Joung D, Zhai L, Das S, Khondaker SI, Seal S. Graphene based materials: past, present and future. Prog Mater Sci. 2011;56(8):1178.
[17] Balandin AA, Ghosh S, Bao WZ, Calizo I, Teweldebrhan D, Miao F, Lau CN. Superior thermal conductivity of single-layer graphene. Nano Lett. 2008;8(3):902.
[18] Estili M, Sakka Y. Recent advances in understanding the reinforcing ability and mechanism of carbon nanotubes in ceramic matrix composites. Sci Technol Adv Mat. 2014;15(6): 064902.
[19] Soldano C, Mahmood A, Dujardin E. Production, properties and potential of graphene. Carbon. 2010;48(8):2127.
[20] Tkalya EE, Ghislandi M, With GD, Koning CE. The use of surfactants for dispersing carbon nanotubes and graphene to make conductive nanocomposites. Curr Opin Colloid Interface Sci. 2012;17(4):225.
[21] Galusek D, Galuskova D. Alumina matrix composites with non-oxide nanoparticle addition and enhanced functionalities. Nanomaterials. 2015;5(1):115.
[22] Aparna R, Sivakumar N, Balakrishnan A, Nair AS, Nair SV, Subramanian KRV. An effective route to produce few-layer graphene using combinatorial ball milling and strong aqueous exfoliants. J Renew Sustain Energy. 2013;5(3):033123.
[23] Li DX, Yang ZH, Jia DC, Duan XM, He PG, Yu J, Zhou Y. Spark plasma sintering and toughening of graphene platelets reinforced SiBCN nanocomposites. Ceram Int. 2015;41(9): 10755.
[24] Kim W, Oh HS, Shon IJ. The effect of graphene reinforcement on the mechanical properties of Al_2O_3 ceramics rapidly sintered by high-frequency induction heating. Int J Refract Met Hard Mater. 2015;48:376.
[25] He T, Li JL, Wang LJ, Zhu JJ, Jiang W. Preparation and consolidation of alumina/graphene composite powders. Mater Trans. 2009;50(4):749.
[26] Fan YC, Wang LJ, Li JL, Li JQ, Sun SK, Chen F, Chen LD, Jiang W. Preparation and electrical properties of graphene nanosheet/Al_2O_3 composites. Carbon. 2010;48(6):1743.
[27] Liu X, Fan YC, Li JL, Wang LJ, Jiang W. Preparation and mechanical properties of graphene nanosheet reinforced alumina composites. Adv Eng Mater. 2015;17(1):28.
[28] Kun P, Tapaszto O, Weber F, Balazsi C. Determination of structural and mechanical properties of multilayer graphene added silicon nitride-based composites. Ceram Int. 2012;38(1): 211.
[29] An XH, Simmons TJ, Shah R, Wolfe C, Lewis KM, Washington M, Nayak SK, Talapatra S, Kar S. Stable aqueous dispersions of noncovalently functionalized graphene from graphite and their multifunctional high-performance applications. Nano Lett. 2010;10(11):4295.
[30] Chintapalli RK, Marro FG, Milsom B, Reece M, Anglada M. Processing and characterization of high-density zirconia–carbon nanotube composites. Mater Sci Eng, A. 2012;549:50.
[31] Low FW, Lai CW, Abd Hamid SB. Easy preparation of ultrathin reduced graphene oxide sheets at a high stirring speed. Ceram Int. 2015;41(4):5798.
[32] López-Pernía C, Muñoz-Ferreiro C, González-Orellana C, Morales-Rodríguez A, Gallardo-López Á, Poyato R. Optimizing the homogenization technique for graphene nanoplatelet/yttria tetragonal zirconia composites: influence on the microstructure and the electrical conductivity. J Alloys Compd. 2018;767(30):994.
[33] Wang L, Bi JQ, Wang WL, Hao XX, Gao XC, Yan WK. The effect of dispersion method on the mechanical properties of graphene reinforced alumina composites. Solid State Phenom. 2018;281:93.
[34] Nieto A, Huang L, Han YH, Schoenung JM. Sintering behavior of spark plasma sintered alumina with graphene nanoplatelet reinforcement. Ceram Int. 2015;41(4):5926.
[35] Porwal H, Tatarko P, Grasso S, Khaliq J, Dlouhy I, Reece MJ. Graphene reinforced alumina nano-composites. Carbon. 2013; 64:359.
[36] Rincon A, Moreno R, Chinelatto ASA, Gutierrez-Gonzalez CF, Rayon E, Salvador MD, Borrell A. Al_2O_3-3YTZP-graphene multilayers produced by tape casting and spark plasma sintering. J Eur Ceram Soc. 2014;34(10):2427.
[37] Yan KL, Fan RH, Chen M, Sun K, Wang XA, Hou Q, Pan SB, Yu MX. An impregnation-reduction method to prepare graphite nanosheet/alumina composites and its high-frequency dielectric properties. Rare Met. 2017;36(3):205.
[38] Yazdani B, Xia YD, Ahmad I, Zhu YQ. Graphene and carbon nanotube (GNT)-reinforced alumina nanocomposites. J Eur Ceram Soc. 2015;35(1):179.
[39] Chen BB, Liu X, Zhao XQ, Wang Z, Wang LJ, Jiang W, Li JL. Preparation and properties of reduced graphene oxide/fused silica composites. Carbon. 2014;77:66.
[40] Wang K, Wang YF, Fan ZJ, Yan J, Wei T. Preparation of graphene nanosheet/alumina composites by spark plasma sintering. Mater Res Bull. 2011;46(2):315.
[41] Fan YC, Kang LJ, Zhou WW, Jiang W, Wang LJ, Kawasaki A. Control of doping by matrix in few-layer graphene/metal oxide composites with highly enhanced electrical conductivity. Carbon. 2015;81:83.
[42] Centeno A, Rocha VG, Alonso B, Fernandez A, Gutierrez-Gonzalez CF, Torrecillas R, Zurutuza A. Graphene for tough and electroconductive alumina ceramics. J Eur Ceram Soc. 2013;33(15–16):3201.
[43] Walker LS, Marotto VR, Rafiee MA, Koratkar N, Corral EL. Toughening in Graphene ceramic composites. ACS Nano. 2011;5(4):3182.
[44] Hintze C, Morita K, Riedel R, Ionescu E, Mera G. Facile sol–gel synthesis of reduced graphene oxide/silica nanocomposites. J Eur Ceram Soc. 2016;36(12):2923.
[45] Mohammad-Rezaei R, Razmi H, Jabbari M. Graphene ceramic composite as a new kind of surface-renewable electrode: application to the electroanalysis of ascorbic acid. Microchim Acta. 2014;181(15–16):1879.
[46] Rice RW, Wu CC, Borchelt F. Hardness grain-size relations in ceramics. J Am Ceram Soc. 1994;77(10):2539.

[47] Zhang SC, Fahrenholtz WG, Hilmas GE, Yadlowsky EJ. Pressureless sintering of carbon nanotube-Al_2O_3 composites. J Eur Ceram Soc. 2010;30(6):1373.
[48] Markandan K, Chin JK, Tan M. Recent progress in graphene based ceramic composites: a review. J Mater Res. 2017;32(1):84.
[49] Fan YC, Wang LJ, Jiang W. Graphene based oxide ceramic composites with high mechanical and functional performance: from preparation to property. J Inorg Mater. 2018;33(2):138.
[50] Grigoriev S, Peretyagin P, Smirnov A, Solis W, Diaz LA, Fernandez A, Torrecillas R. Effect of graphene addition on the mechanical and electrical properties of Al_2O_3-SiC_w ceramics. J Eur Ceram Soc. 2017;37(6):2473.
[51] Tapasztó O, Puchy V, Horváth ZE, Fogarassy Z, Bódis E, Károly Z, Balázsi K, Dusza J, Tapasztó L. The effect of graphene nanoplatelet thickness on the fracture toughness of Si_3N_4 composites. Ceram Int. 2019;45(6):6858.
[52] Liu J, Guo HK, Su Y, Wang LB, Wei L, Yang G, Yang Y, Jiang KL. Spark plasma sintering of graphene platelet reinforced zirconia composites with improved mechanical performance. Mater Sci Eng, A. 2017;688:70.
[53] Lahiri D, Khaleghi E, Bakshi SR, Li W, Olevsky EA, Agarwal A. Graphene-induced strengthening in spark plasma sintered tantalum carbide–nanotube composite. Scr Mater. 2013;68(5):285.
[54] Tapaszto O, Kun P, Weber F, Gergely G, Balazsi K, Pfeifer J, Arato P, Kidari A, Hampshire S, Balazsi C. Silicon nitride based nanocomposites produced by two different sintering methods. Ceram Int. 2011;37(8):3457.
[55] Huang H, Chen W, Chen S, Wee ATS. Bottom-up growth of epitaxial graphene on 6H-SiC(0001). ACS Nano. 2008;2(12):2513.
[56] Park J, Mitchel WC, Grazulis L, Smith HE, Eyink KG, Boeckl JJ, Tomich DH, Pacley SD, Hoelscher JE. Epitaxial graphene growth by carbon molecular beam epitaxy (CMBE). Adv Mater. 2010;22(37):4140.
[57] Yannopoulos SN, Siokou A, Nasikas NK, Dracopoulos V, Ravani F, Papatheodorou GN. CO_2 laser-induced growth of epitaxial graphene on 6HSiC (0001). Adv Funct Mater. 2012;22(1):113.
[58] Antonelou A, Dracopoulos V, Yannopoulos SN. Laser processing of SiC: from graphene-coated SiC particles to 3D graphene froths. Carbon. 2015;85:176.
[59] Miranzo P, Ramirez C, Roman-Manso B, Garzon L, Gutierrez HR, Terrones M, Ocal C, Osendi MI, Belmonte M. In situ processing of electrically conducting graphene/SiC nanocomposites. J Eur Ceram Soc. 2013;33(10):1665.
[60] So-Mang Kwon, Seok-Jae Lee, In-Jin Shon. Enhanced properties of nanostructured ZrO_2-graphene composites rapidly sintered via high-frequency induction heating. Ceram Int. 2015;41(1):835.
[61] Ahmad I, Islam M, Abdo HS, Subhani T, Khalil KA, Almajid AA, Yazdani B, Zhu YQ. Toughening mechanisms and mechanical properties of graphene nanosheet-reinforced alumina. Mater Des. 2015;88:1234.
[62] Fan YC, Estili M, Igarashi G, Jiang W, Kawasaki A. The effect of homogeneously dispersed few-layer graphene on microstructure and mechanical properties of Al_2O_3 nanocomposites. J Eur Ceram Soc. 2014;34(2):443.
[63] Liu J, Yan HX, Reece MJ, Jiang K. Toughening of zirconia/alumina composites by the addition of graphene platelets. J Eur Ceram Soc. 2012;32(16):4185.
[64] Liu J, Yan HX, Jiang K. Mechanical properties of graphene platelet-reinforced alumina ceramic composites. Ceram Int. 2013;39(6):6215.
[65] Liu J, Li Z, Yan HX, Jiang KL. Spark plasma sintering of alumina composites with Graphene platelets and silicon carbide nanoparticles. Adv Eng Mater. 2014;16(9):1111.
[66] Fan YC, Igarashi G, Jiang W, Wang LJ, Kawasaki A. Highly strain tolerant and tough ceramic composite by incorporation of graphene. Carbon. 2015;90:274.
[67] Kim HJ, Lee SM, Oh YS, Yang YH, Lim YS, Yoon DH, Lee C, Kim JY, Ruoff RS. Unoxidized Graphene/alumina nanocomposite: fracture- and wear-resistance effects of Graphene on alumina matrix. Sci Rep-UK. 2014;4:5176.
[68] Liu J, Yang Y, Hassanin H, Jumbu N, Deng SA, Zuo Q, Jiang KL. Graphene-alumina nanocomposites with improved mechanical properties for biomedical applications. ACS Appl Mater Inter. 2016;8(4):2607.
[69] Del Rio F, Boado MG, Rama A, Guitian F. A comparative study on different aqueous-phase graphite exfoliation methods for few-layer graphene production and its application in alumina matrix composites. J Eur Ceram Soc. 2017;37(12):3681.
[70] Ahmad I, Islam M, Subhani T, Zhu YQ. Toughness enhancement in graphene nanoplatelet/SiC reinforced Al_2O_3 ceramic hybrid nanocomposites. Nanotechnology. 2016;27(42):425704.
[71] Jiang KL, Li JR, Liu J. Spark plasma sintering and characterization of Graphene platelet/ceramic composites. Adv Eng Mater. 2015;17(5):716.
[72] Llorente J, Roman-Manso B, Miranzo P, Belmonte M. Tribological performance under dry sliding conditions of graphene/silicon carbide composites. J Eur Ceram Soc. 2016;36(3):429.
[73] Belmonte M, Ramirez C, Gonzalez-Julian J, Schneider J, Miranzo P, Osendi MI. The beneficial effect of graphene nanofillers on the tribological performance of ceramics. Carbon. 2013;61:431.
[74] Tapaszto O, Balko J, Puchy V, Kun P, Dobrik G, Fogarassy Z, Horvath ZE, Dusza J, Balazsi K, Balazsi C, Tapaszto L. Highly wear-resistant and low-friction Si_3N_4 composites by addition of graphene nanoplatelets approaching the 2D limit. Sci Rep-UK. 2017;7(1):10087.
[75] Seiner H, Sedlak P, Koller M, Landa M, Ramirez C, Osendi MI, Belmonte M. Anisotropic elastic moduli and internal friction of graphene nanoplatelets/silicon nitride composites. Compos Sci Technol. 2013;75:93.
[76] Koller M, Seiner H, Landa M, Nieto A, Agarwal A. Anisotropic elastic and acoustic properties of bulk Graphene nanoplatelets consolidated by spark plasma sintering. Acta Phys Pol, A. 2015;128(4):670.
[77] Rutkowski P, Stobierski L, Zientara D, Jaworska L, Klimczyk P, Urbanik M. The influence of the graphene additive on mechanical properties and wear of hot-pressed Si_3N_4 matrix composites. J Eur Ceram Soc. 2015;35(1):87.
[78] Tapaszto O, Tapaszto L, Lemmel H, Puchy V, Dusza J, Balazsi C, Balazsi K. High orientation degree of graphene nanoplatelets in silicon nitride composites prepared by spark plasma sintering. Ceram Int. 2016;42(1):1002.
[79] Cheng YH, Lyu Y, Han WB, Hu P, Zhou SB, Zhang XH. Multiscale toughening of ZrB_2-SiC-Graphene@ZrB_2-SiC dual composite ceramics. J Am Ceram Soc. 2019;102(4):2041.
[80] Zhang C, Boesl B, Silvestroni L, Sciti D, Agarwal A. Deformation mechanism in graphene nanoplatelet reinforced tantalum carbide using high load in situ indentation. Mater Sci Eng A-Struct. 2017;674(30):270.
[81] Yadhukulakrishnan GB, Karumuri S, Rahman A, Singh RP, Kalkan AK, Harimkar SP. Spark plasma sintering of graphene reinforced zirconium diboride ultra-high temperature ceramic composites. Ceram Int. 2013;39(6):6637.
[82] Asl MS, Kakroudi MG. Characterization of hot-pressed graphene reinforced ZrB_2–SiC composite. Mater Sci Eng, A. 2015;625:385.

[83] Nieto A, Lahiri D, Agarwal A. Graphene nanoplatelets reinforced tantalum carbide consolidated by spark plasma sintering. Mater Sci Eng, A. 2013;582:338.
[84] Hashemi R, Weng GJ. A theoretical treatment of graphene nanocomposites with percolation threshold, tunneling-assisted conductivity and microcapacitor effect in AC and DC electrical settings. Carbon. 2016;96:474.
[85] Qing YC, Wen QL, Luo F, Zhou WC. Temperature dependence of the electromagnetic properties of graphene nanosheet reinforced alumina ceramics in the X-band. J Mater Chem C. 2016;4(22):4853.
[86] Lee E, Choi KB, Lee SM, Kim JY, Jung JY, Baik SW, Lim YS, Kim SJ, Shim W. A scalable and facile synthesis of alumina/exfoliated graphite composites by attrition milling. RSC Adv. 2015;5(113):93267.
[87] Fan YC, Jiang W, Kawasaki A. Highly conductive few-layer graphene/Al_2O_3 nanocomposites with tunable charge carrier type. Adv Funct Mater. 2012;22(18):3882.
[88] Rutkowski P, Klimczyk P, Jaworska L, Stobierski L, Dubiel A. Thermal properties of pressure sintered alumina-graphene composites. J Therm Anal Calorim. 2015;122(1):105.
[89] Celik Y, Celik A, Flahaut E, Suvaci E. Anisotropic mechanical and functional properties of graphene-based alumina matrix nanocomposites. J Eur Ceram Soc. 2016;36(8):2075.
[90] Zong PA, Hanus R, Dylla M, Tang YS, Liao JC, Zhang QH, Snyder GJ, Chen LD. Skutterudite with graphene-modified grain-boundary complexion enhances ZT enabling high-efficiency thermoelectric device. Energy Environ Sci. 2017;10(1):183.
[91] Lin CJ, Lin IC, Tuan WH. Effect of graphene concentration on thermal properties of alumina-graphene composites formed using spark plasma sintering. J Mater Sci. 2017;52(3):1759.
[92] Chen C, Pan LM, Li XY, Zhang JX, Feng YB, Yang J. Mechanical and thermal properties of graphene nanosheets/magnesia composites. Ceram Int. 2017;43(13):10377.
[93] Ramirez C, Garzon L, Miranzo P, Osendi MI, Ocal C. Electrical conductivity maps in graphene nanoplatelet/silicon nitride composites using conducting scanning force microscopy. Carbon. 2011;49:3873.
[94] Ramirez C, Figueiredo FM, Miranzo P, Poza P, Osendi MI. Graphene nanoplatelet/silicon nitride composites with high electrical conductivity. Carbon. 2012;50:3607.
[95] Roman-Manso B, Domingues E, Figueiredo FM, Belmonte M, Miranzo P. Enhanced electrical conductivity of silicon carbide ceramics by addition of graphene nanoplatelets. J Eur Ceram Soc. 2015;35(10):2723.
[96] Tan YQ, Luo H, Zhang HB, Peng SM. Graphene nanoplatelet reinforced boron carbide composites with high electrical and thermal conductivity. J Eur Ceram Soc. 2016;36(11):2679.
[97] Sedlak R, Kovalcikova A, Mudra E, Rutkowski P, Dubiel A, Girman V, Bystricky R, Dusza J. Boron carbide/graphene platelet ceramics with improved fracture toughness and electrical conductivity. J Eur Ceram Soc. 2017;37(12):3773.
[98] Miranzo P, Garcia E, Ramirez C, Gonzalez-Julian J, Belmonte M, Osendi MI. Anisotropic thermal conductivity of silicon nitride ceramics containing carbon nanostructures. J Eur Ceram Soc. 2012;32(8):1847.
[99] Roman-Manso B, Chevillotte Y, Osendi MI, Belmonte M, Miranzo P. Thermal conductivity of silicon carbide composites with highly oriented graphene nanoplatelets. J Eur Ceram Soc. 2016;36(16):3987.
[100] Simsek ING, Nistal A, Garcia E, Perez-Coll D, Miranzo P, Osendi MI. The effect of graphene nanoplatelets on the thermal and electrical properties of aluminum nitride ceramics. J Eur Ceram Soc. 2017;37(12):3721.

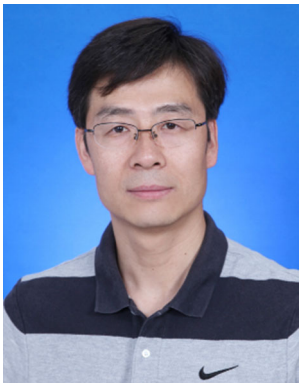

Lian-Jun Wang is a full professor in the College of Material Science and Engineering at Donghua University. He received his Ph.D. in chemical engineering from Dalian University of Technology in 2002. He carried out postdoctoral research at Shanghai Institute of Ceramics, Chinese Academy of Sciences (2002–2004) and Stockholm University (2007–2008). His research interests focus on the study and development of new sintering technologies, the design and controlled fabrication of bulk nanocomposites and their applications. He has published over 100 scientific papers in SCI Journals, including Nat. Commun., Adv. Mater., Adv. Energy Mater., Adv. Funct. Mater., ACS Nano, Nano Energy, etc. Besides, he participated in the writing of 3 books and gained over 20 patents.